

## Review

### Conversion of brain cytosol profile from fetal to adult type during the perinatal period: Taurine-NAA exchange

By Tsutomu NAKADA<sup>\*1,†</sup>

(Communicated by Takashi SUGIMURA, M.J.A.)

**Abstract:** Mammals face drastic environmental changes at birth. Appropriate adjustments of various systems must take place rapidly to accommodate this once in a life time event. The brain undergoes significant adjustments as well, the most obvious of which is in its need to meet the drastic increase in energy consumption at the neuronal cell membrane due to the explosive increase in neural activities after birth. Actual changes were found to be taken place in two systems, namely, acid base balance control and cytosolic energy transport. The adjustments are accomplished by converting cytosol microenvironment from a taurine rich fetal type environment to an N-acetyl-aspartate (NAA) rich adult type environment during the post-natal period. High concentrations of taurine are necessary to provide effective buffering in the fetal brain, because the fetus cannot utilize the adult type of pCO<sub>2</sub> dependent acid–base balance control system, namely respiration driven pCO<sub>2</sub> changes. To accommodate the significantly higher demand of energy consumption at the membrane due to the increased neuronal activities, taurine has to be replaced by NAA, since the latter facilitates HEP transport from mitochondria to the membrane by passive diffusion.

**Keywords:** taurine, N-acetyl-aspartate, NAA, diffusion, high energy phosphate, fetus

#### Background

Mammals face drastic environmental changes at birth. Appropriate adjustments of various systems must take place rapidly to accommodate this once in a life time event.<sup>1)</sup> The perinatal adjustment processes of the circulatory and respiratory systems are well known examples. The adjustment processes the central nervous system (CNS), on the other hand, had been underrecognized. The brain undergoes significant adjustments post-natally, the most obvious of which is its need to meet the drastic increase in energy consumption at the neuronal cell membrane due to the explosive increase in neural activities after birth.

Essentially instantaneous conversion occurs at birth for purely physical systems such as the circulatory system. By contrast, for systems that

rely on biological materials, a gradual replacement of substrates takes place, a well known example of which being the hemoglobin system. The early post-natal period represents a critical transition time for conversion from fetal life to adult life.

Various efforts have been made for the proper investigation of energy kinetics in the brain and have resulted in the development of many sophisticated brain fixation methods, such as the freeze-blow technique. Nevertheless, no method was fast enough to completely eliminate artificial changes associated with anoxia/ischemia during fixation. It became clear that development of non-invasive quantitative analysis of the brain *in vivo* was essential to accurately investigate the kinetic parameters of brain cellular energetics. Magnetic resonance spectroscopy (MRS) is thus far the sole technique capable of performing such analyses.<sup>2)–4)</sup>

Using various advanced MRS techniques, we found that changes in the cytosolic microenvironment play a key role in post-natal adjustment.<sup>5)–29)</sup> Taurine, a free cytosolic amino acid rich in fetal brain is central in the fetal type of acid–base balance control system (taurine buffer). Taurine also,

<sup>\*1</sup> Professor, Brain Research Institute, University of Niigata, Niigata, Japan.

<sup>†</sup> Correspondence should be addressed: T. Nakada, M.D., Ph.D., FAAN, Center for Integrated Human Brain Science, Brain Research Institute, University of Niigata, 1 Asahimachi, Chuohku, Niigata 951-8585, Japan (e-mail: tnakada@bri.niigata-u.ac.jp).

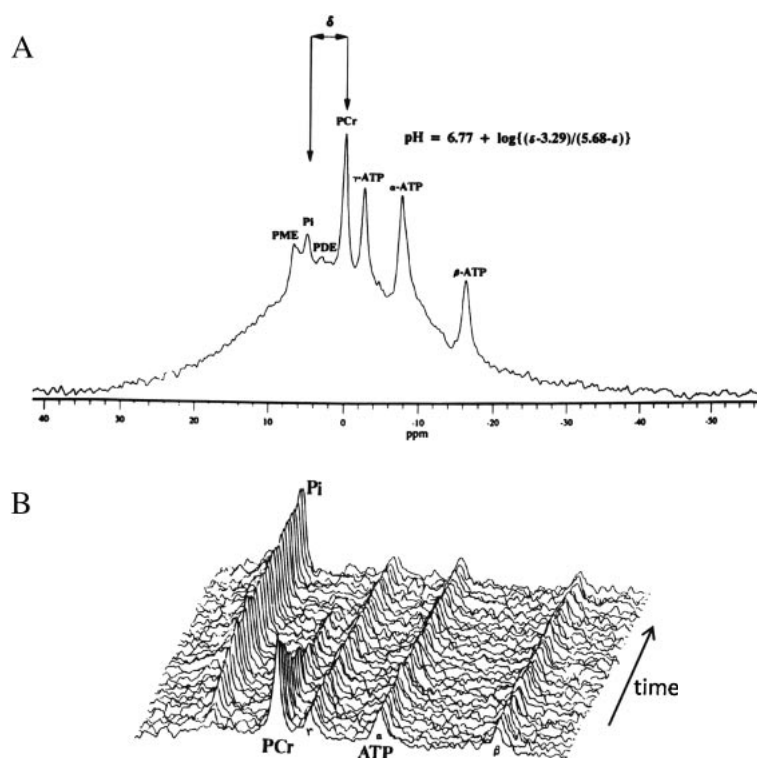


Fig. 1.  $^{31}\text{P}$  MRS of adult rat brain.

A: Seven resonances are typically resolvable. PCr: phosphocreatine;  $\alpha$ -,  $\beta$ -,  $\gamma$ -ATP; Pi: inorganic phosphate; PM: phosphomonoester; PD: phosphodiester. Chemical shift of Pi relative to PCr is pH dependent and, therefore, can be used to estimate intracellular pH. Note: seven clearly resolved resonances are on the large hump which represents the sum of small, wide (short T2), resonances from other cellular components.

B: Stack plot showing continuous monitoring of cellular energy state following ischemia. Note: the rapid decline in PCr and increase in Pi.

however, retards cytosolic high energy phosphate (HEP) transport. In early post-natal life, taurine is rapidly replaced by another cytosolic free amino acid, N-acetyl-aspartate (NAA) to facilitate HEP transport.

#### Methodological consideration

**$^{31}\text{P}$  MRS.** A typical *in vivo*  $^{31}\text{P}$  spectrum of the brain consists of seven resonances:  $\alpha$ -,  $\beta$ - and  $\gamma$ -ATP, phosphocreatine (PCr), inorganic phosphate (Pi), phosphomonoester (PME), and phosphodiester (PDE) (Fig. 1A). Five of the seven resonances of the  $^{31}\text{P}$  spectrum are related to the molecules responsible for cellular energetics, namely, ATP, PCr, and Pi. Quantitative monitoring of  $^{31}\text{P}$  spectra, therefore, allows for accurate assessment of cellular energetics (Fig. 1B). The remaining two resonances represent primarily precursor (PME) and catabolic metabolites (PDE) of membrane phospholipids. Quantification of PME and PDE provide indirect

information regarding membrane phospholipid metabolism.<sup>2)-6),8),10),11)</sup>

Another important application of  $^{31}\text{P}$  MRS is the assessment of intracellular pH. This is possible because certain resonance frequencies are pH dependent. The most widely utilized method makes use of changes in the chemical shift of the Pi resonance with respect to the PCr resonance (Fig. 1A).

**$^1\text{H}$  (proton) MRS.** Detection of signals of substrates from among the overwhelmingly strong signals of water and fat (which are utilized in MRI) requires special technical manipulation termed solvent or water suppression.<sup>8)-10),12),13)</sup> Resonances easily resolvable in the normal adult brain using this technique include choline (Cho), creatine (Cre), and N-acetyl-aspartate (NAA) (Fig. 2A). Glutamate, glutamine and  $\gamma$ -amino butyric acid (GABA), compounds of high biological importance, are other resolvable resonances, albeit the detection of which is more technically demanding. Lactate, the

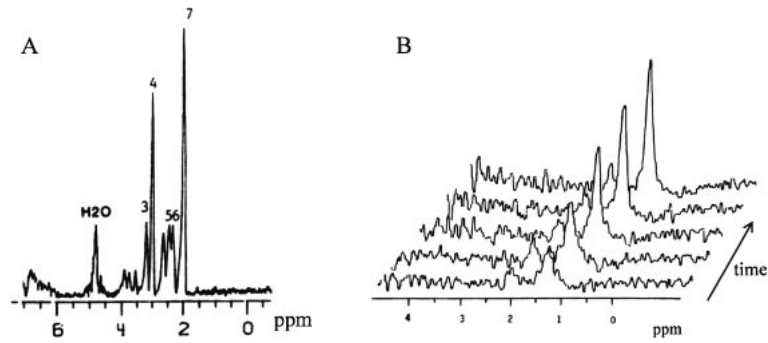


Fig. 2. Proton MRS of adult rat brain.

A: Typically resolvable resonances include choline (3), creatine (4), and N-acetyl aspartate (NAA) (7). Glutamine, glutamate, and  $\gamma$ -amino butyric acid (GABA) creates compound resonances, generally referred to as Glx (5, 6). H<sub>2</sub>O: residual water signals.  
 B: Stack plot showing accumulation of lactate associated anoxia.

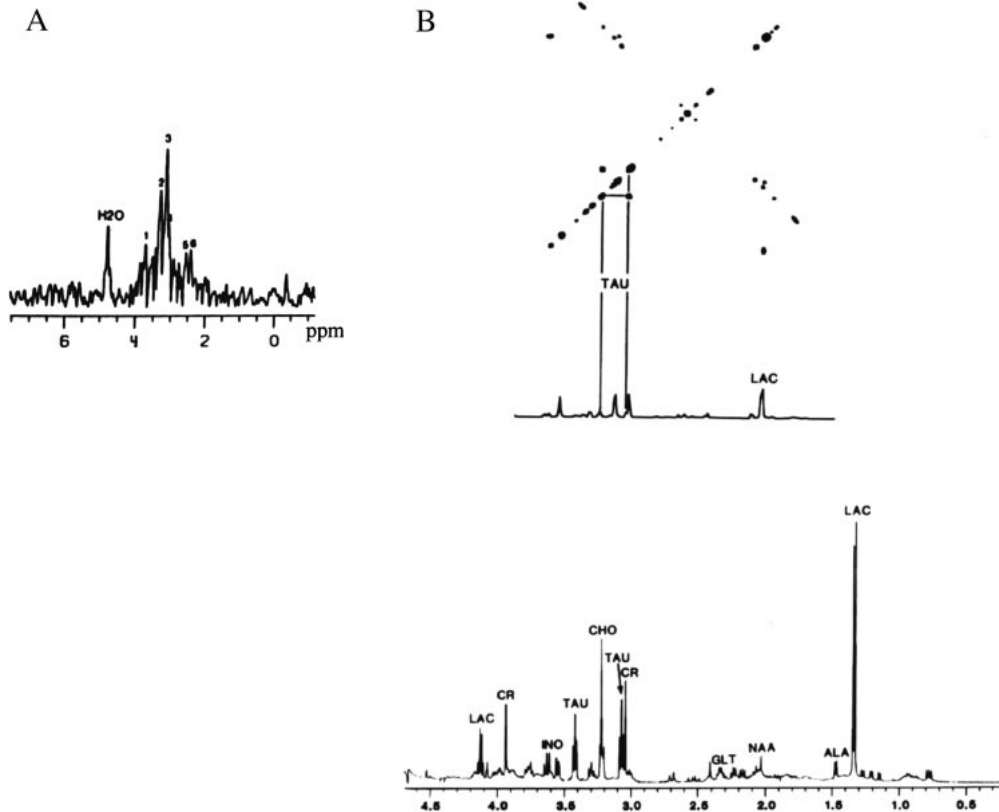


Fig. 3. Proton MRS of fetal brain.

A: *In vivo* proton MRS of fetal brain (21st gestational day) showed choline (3) and creatine (4) and GLX (5, 6), but virtually no NAA. Additionally, the very prominent peak of taurine (2) is clearly resolved. Another resonance resolved is inositol (1). H<sub>2</sub>O: residual water signals.

B: Taurine shift assignment confirmation processes. High resolution spectrum of fetal brain perchloric acid extract of 21st day fetal brain (lower) showed two triplets of the taurine resonance at 3.07 and 3.43 ppm. COSY experiment (upper) showed coupling of two taurine triplets and confirmed the shift assignment. LAC: lactate, CR: creatine, TAU: taurine, INO: inositol, GLT: glutamine, NAA: N-acetyl-aspartate, ALA: alanine. A singlet at 2.41 ppm is succinate. Chemical shifts were referred to an internal TMS reference at 0.0 ppm.

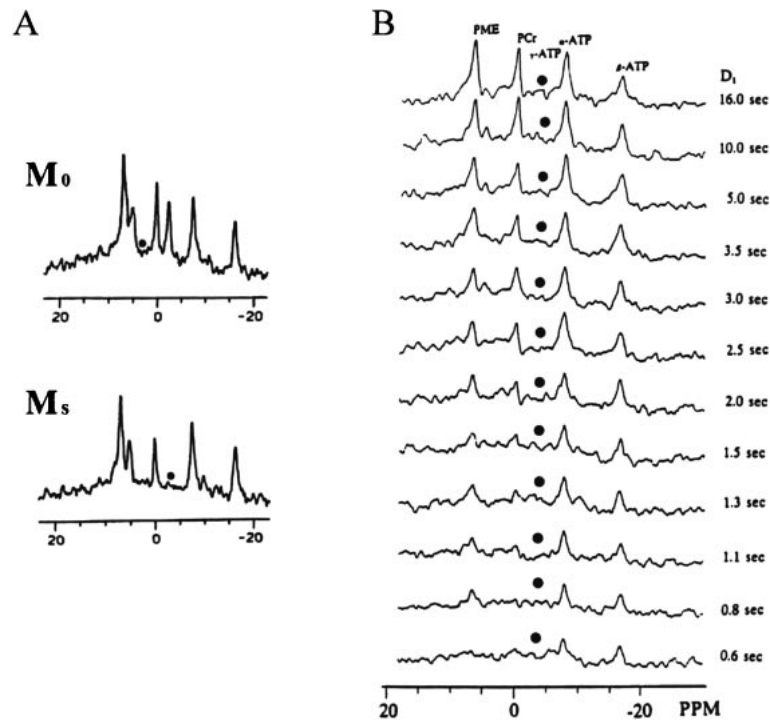


Fig. 4.  $^{31}\text{P}$  saturation transfer experiments of newborn pup.

A:  $M_0$  and  $M_s$  measurement. Dots denote the frequency at which saturation pulse was applied.  $M_0$ : reference spectrum for  $\gamma$ -ATP saturation;  $M_s$ :  $\gamma$ -ATP saturation.

B:  $T_{1\text{app}}$  determination. Dots denote the frequency at which saturation pulse was applied.

product of anaerobic glycolysis, represents another substrate of interest (Fig. 2B). In the fetus, another amino acid, taurine, is present in high concentration (Fig. 3).<sup>10),14),27),30),31)</sup>

**High energy phosphate (HEP) life span measurement.** Creatine kinase (CK) is the enzyme which catalyzes the reaction:



where PCr is phosphocreatine, ADP is adenosine diphosphate, ATP is adenosine triphosphate, and Cr is creatine. Although the precise role of CK in cellular energy metabolism is not fully understood, it has been postulated that PCr acts as either a high energy reservoir (ATP buffer) or an energy shuttle between the mitochondria and cytoplasm (PCr shuttle). The saturation transfer (ST) experiment is a steady-state NMR magnetization transfer technique capable of measuring the rate of chemical exchanges. The rate of enzyme mediated biochemical reactions can be measured *in vivo* using this technique.<sup>32)-37)</sup> CK catalyzes the above reaction bi-directionally and the reaction *in vivo* is believed to be near equilibrium. The resonances of the intermediary metabolites in

this reaction, namely, PCr, ATP, and Pi, can be readily detected by  $^{31}\text{P}$  MRS. Therefore, this "contained" enzymatic reaction is suitable for  $^{31}\text{P}$  NMR saturation transfer experiments.

The pseudo-first order rate constants can be determined using the equation:

$$K = [1 - M_s/M_0]/T_{1\text{app}}$$

where K is the rate constant,  $M_0$  is the magnetization without saturation on the exchanging partner,  $M_s$  is the magnetization with saturation on the exchanging partner, and  $T_{1\text{app}}$  is the apparent  $T_1$  measured with saturation on the exchanging partner (Fig. 4).

The intracellular level of PCr,  $[\text{PCr}]$ , can be given by:

$$[\text{PCr}] = [\text{ATP}] \times H_{p/a}$$

where  $H_{p/a}$  is the ratio of the Lorentzian corrected heights of the PCr and ATP resonances obtained from a fully relaxed  $^{31}\text{P}$  spectrum. Since the creatine kinase (CK) reaction is the sole reaction for PCr and the flux of the steady state CK reaction is at least equal to the maximum steady state turnover rate of ATP, it is possible to calculate the shortest life span

of PCr and ATP by:

$$\text{PCr life span} = \frac{[\text{PCr}]}{\text{flux}} = \frac{[\text{PCr}]}{[\text{PCr}] \times K} = \frac{1}{K}$$

$$\text{ATP life span} = \frac{[\text{ATP}]}{\text{flux}} = \frac{[\text{ATP}]}{[\text{PCr}] \times K} = \frac{1}{H_{p/a} \times K}$$

**HEP Diffusivities measurement.** Intracellular transport of HEP is purely dependent on the passive diffusion through the cytosol. In mammalian brain, ATP is primarily produced in the mitochondria by oxidative phosphorylation and transported to the plasma membrane where it is utilized to maintain membrane excitability. Accordingly, HEP diffusivities can provide significant information on the cytosolic microenvironment *in vivo*. MRS represents the sole technique capable of providing such information.<sup>21),22),29)</sup>

Fick's law for particle flux density is given by:

$$\mathbf{J} = D\nabla n$$

where  $D$  is the diffusion coefficient and  $n$  is the concentration of the particle. The equation of continuity,

$$\frac{\partial n}{\partial t} + \nabla \cdot \mathbf{J} = 0$$

assures that the number of particles is conserved. The diffusion equation is then given by,

$$\frac{\partial n}{\partial t} = D\nabla^2 n$$

where  $\nabla^2$  represents the Laplacian.<sup>38),39)</sup>

The canonical solution to the diffusion equation is a normalized Gaussian function, which in one dimension (x-component) can be expressed as,

$$\theta(x, t) = \frac{1}{\sqrt{4\pi D_x t}} \exp\left(-\frac{x^2}{4D_x t}\right).$$

By evaluating the Gaussian integral, it becomes apparent that the mean square value of  $x$  can be expressed simply by,

$$\langle x_{(t)}^2 \rangle = 2D_x t,$$

and in turn, the root mean square value by,

$$x_{rms} = \sqrt{\langle \bar{x}_{(t)}^2 \rangle} = \sqrt{2D_x t}.$$

In physical realism, this value can be treated as the statistical average distance traveled by the particle in one dimension (Fig. 5A). The relationship between the Gaussian function and  $x_{rms}$  is graphically presented in Fig. 1. Here, dispersion occurs with time along with a mean distance of  $\sqrt{2Dt}$ .

It is apparent that, in three-dimensional diffusion, the diffusion coefficient  $D$  has to be given in a second order tensor  $\mathbf{D}^\xi$ , which can be expressed in the form of,

$$\mathbf{D}^\xi = \begin{pmatrix} \lambda_1 & 0 & 0 \\ 0 & \lambda_2 & 0 \\ 0 & 0 & \lambda_3 \end{pmatrix}$$

with three eigenvalues of  $\lambda_1 > \lambda_2 > \lambda_3$ , where ellipsoid expression can provide "intuitive" impression of physical realism of molecular diffusion (Fig. 5B). Here, ellipsoid can be seen as the three-dimensional distribution of particles at time  $t$ , all of which are initially located at the origin. To define ellipsoid, the direction of the principal axes and magnitude at each principal axis need to be given. The former corresponds to eigenvector,  $|\lambda\rangle$ , whereas the latter to eigenvalue,  $\lambda$ .

Taking into account the condition where translational micromobility of water molecules possesses orientational dependency (*anisotropic motion*), the signal intensity,  $I$ , of a given pixel in the presence of gradient pulses obtained using a spin echo diffusion weighted imaging (Stejskal & Tanner) sequence (Fig. 5C)<sup>40)</sup> can be expressed as:

$$I = I_{(\infty,0,0)} \cdot \left(1 - 2 \exp\left[-\frac{(T_r - T_e/2)}{T_1}\right] + \exp\left[-\frac{T_r}{T_1}\right]\right) \cdot \exp\left[-\frac{T_e}{T_2}\right] \cdot \exp\left[-\gamma^2 \mathbf{G}^T \mathbf{D}^\xi \mathbf{G} \delta^2 \left(\Delta - \frac{\delta}{3}\right)\right],$$

where  $I_{(\infty,0,0)}$  is the intensity value for  $T_r = \infty$ ,  $T_e = 0$ ,  $|\mathbf{G}|^2 = 0$ ; and  $T_r$  represents repetition time;  $T_e$ , echo time;  $T_1$ , longitudinal relaxation time;  $T_2$ , spin-spin relaxation time;  $\gamma$ , nuclear gyromagnetic ratio;  $\mathbf{D}^\xi$ , diffusion tensor;  $\mathbf{G}$  and  $\mathbf{G}^T$ , gradient vector matrix and its transpose;  $\delta$ , pulse duration; and  $\Delta$ , interval between the gradient pulses. In *in vivo* studies,  $\mathbf{D}^\xi$  is replaced by the apparent diffusion tensor,  $\mathbf{D}_{app}^\xi$ , which, in addition to pure diffusion, includes the effects of other factors which cause intravoxel phase dispersion, such as axoplasmic flow.<sup>40)-43)</sup>

Utilizing closure relationship of  $\sum_i |u_i\rangle \langle u_i|$ , the scalar product,  $\langle \mathbf{G} | \mathbf{D}_{app}^\xi | \mathbf{G} \rangle$  can be expressed as

$$\begin{aligned} \langle \mathbf{G} | \mathbf{D}_{app}^\xi | \mathbf{G} \rangle &= \sum_{i,j} \langle \mathbf{G} | u_i \rangle \langle u_i | \mathbf{D}_{app}^\xi | u_j \rangle \langle u_j | \mathbf{G} \rangle \\ &= \sum_{i,j} \mathbf{G}_i^* \mathbf{D}_{i,j} \mathbf{G}_j \end{aligned}$$

where asterisk signifies the conjugate. This equation signifies that by applying the appropriate combination of gradients, all the matrix components can be

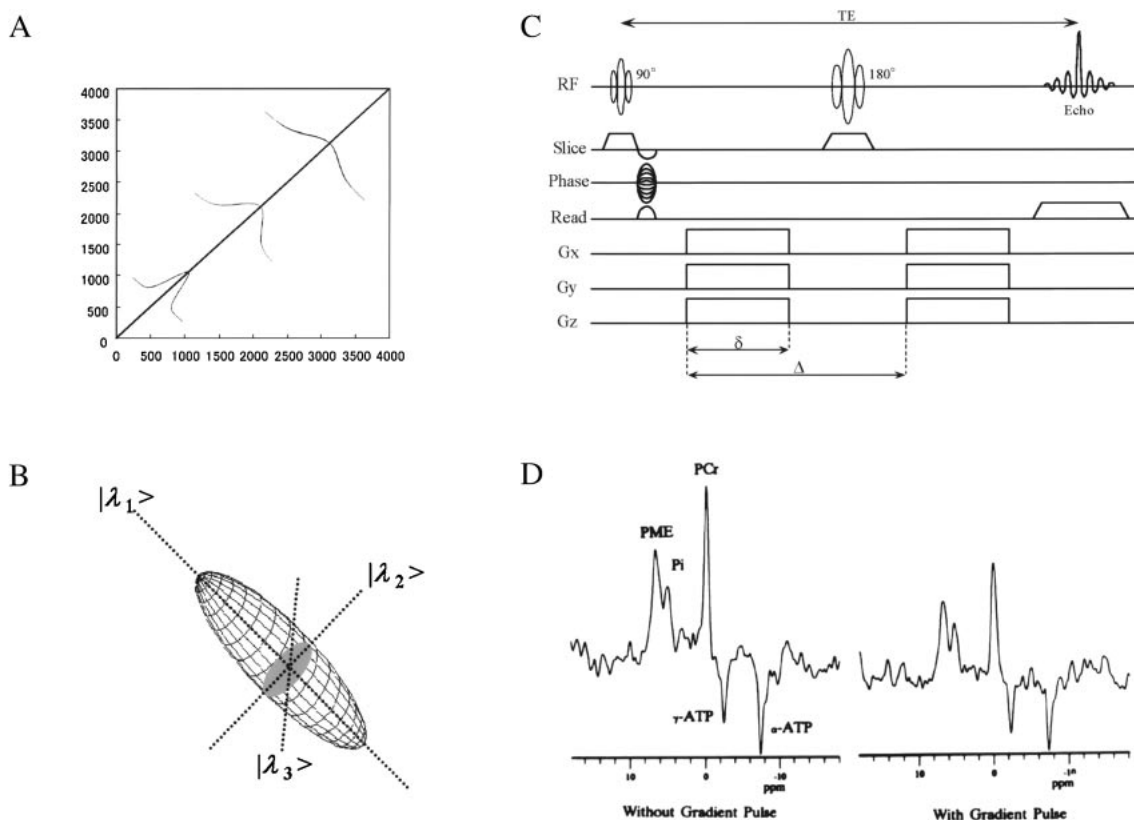


Fig. 5. Diffusivity analysis.

A: Pictorial presentation of physical realism in one dimension.

B: Ellipsoid presentation.

C: Stejskal &amp; Tanner sequence.

D: Representative spectra of  $^{31}\text{P}$  diffusion spectroscopy of newborn pup without and with 10 msec gradient pulse. Note the  $180^\circ$  phase modulation for  $\alpha$ - and  $\gamma$ -ATP due to P-P scalar coupling. Signal intensity of  $\beta$ -ATP (triplet) was significantly attenuated due to phase modulation with the chosen echo time.

effectively extracted into a set of linear equations and, in turn, all the matrix components can be determined. Since the diffusion tensor contains six independent matrix elements, including zero gradients, a minimum of seven images have to be obtained for their determination (Fig. 5D).

### Experimental results

**Taurine-NAA exchange.** Non-invasive steady state MRS spectral analysis of rat brain clearly demonstrates drastic transitional changes in the cytosolic microenvironment, from fetal to adult pattern, during the first 28 days of post-natal life, highly consistent with the results of previous *invasive* studies.  $^{31}\text{P}$  MRS shows significant changes in PCr and PME (Fig. 6), with PCr increasing linearly from the late fetal period (18th gestational day) and through the 28 days of the post-natal period, at

which point it reaches adult levels. Interestingly, this increase in PCr parallels the increase in energy demand of the adult brain. Changes in PME, which represents precursors of membrane phospholipids, correlate closely to the time course of membrane production as represented by choline signals in proton MRS (not shown). Most noteworthy, however, is the inverse correlation of taurine and NAA concentrations as detected using proton MRS (Fig. 7A), an observation referred to here as taurine-NAA exchange.<sup>1),10),14),27),30),31),44)</sup>

Taurine and NAA share surprisingly similar unique characteristics. Taurine and NAA are the only amino acids that exist as free amino acids in the cytosol. Both taurine and NAA are virtually metabolically inert, strongly implying that the role of taurine and NAA in cytosol is physicochemical, rather than biochemical in nature.

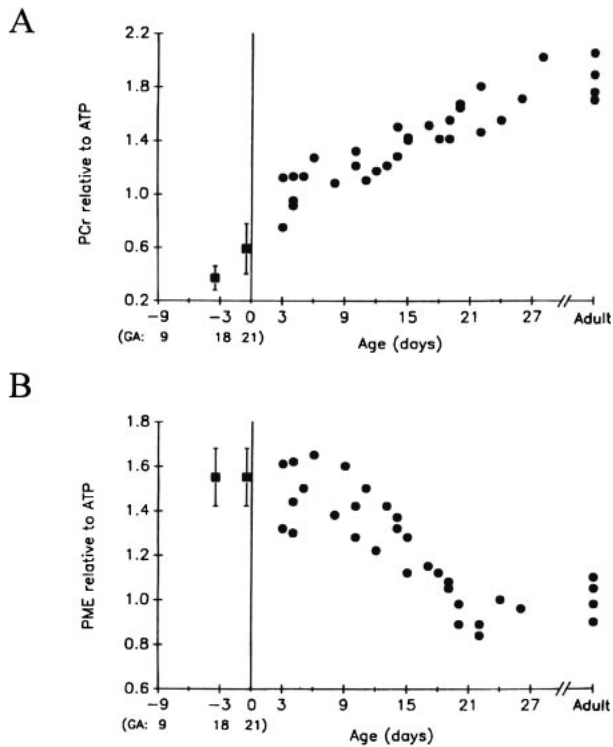


Fig. 6. Perinatal changes in  $^{31}\text{P}$  MRS.

Summary of *in vivo* data obtained non-invasively from early gestational day fetal brain to adults. A: PCr; B: PME.

Given that taurine and NAA are free amino acids in the cytosol, they both participate in cellular ionic balance as major anions. As can be predicted stoichiometrically, the observed changes in taurine and NAA concentrations observed during the early post-natal period occur in a two to one ratio, reflecting their respective molecular anionic charges (Fig. 7B).

These findings provide the first conclusion: *Taurine in fetal brain is the counterpart of NAA in adult brain. During early post-natal life, the chemical microenvironment of the neuronal cytosol undergoes conversion from a taurine rich environment (fetal type) to NAA profile (adult type).*

**Fetal type pH control system: taurine buffer.** Maintenance of normal pH is a biologic requisite. Acid–base balance is, therefore, narrowly controlled. In adult life, it is primarily achieved by the carbonate buffering system. At physiological pH of 7.4, carbonate ( $\text{CO}_3^{2-}$ ) levels are negligible and, therefore, cytosolic carbonate is either in the form of carbonic acid ( $\text{H}_2\text{CO}_3$ ) or bicarbonate ( $\text{HCO}_3^-$ ). Titration studies have shown the pKa value of carbonic acid/bicarbonate solutions under physiological conditions,

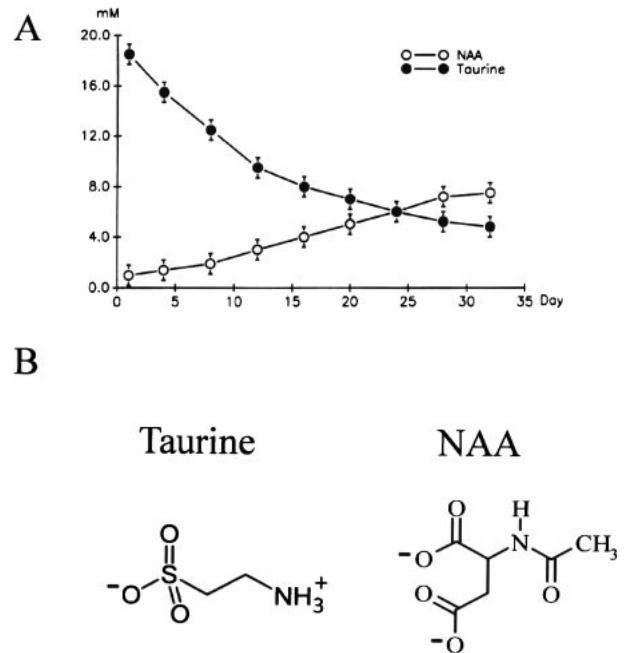


Fig. 7. Taurine-NAA exchange.

A: Summary of *in vivo* proton MRS data for taurine and NAA. Note: inversely correlated changes.

B: Taurine and NAA.

$\text{pCO}_2$  of 40 mmHg, temperature  $37^\circ\text{C}$ , to be 6.12. It is apparent that carbonate itself is not an optimal buffer at physiological pH. Despite its less than optimal pKa value for buffering at physiological pH, the carbonate system has one critical advantage for biological systems, namely, rapid adjustment of carbonic acid levels by manipulation of  $\text{pCO}_2$ . Metabolic acidosis brought about by excess acid formation is quickly compensated by a decrease in  $\text{pCO}_2$  through hyperventilation. This rapid response by means of respiration is a notably efficient and accurate system for acid–base control. Unfortunately, the fetus *in utero* cannot take advantage of this rapid adjustment system. It appears that the fetus *in utero* should have an alternative means for maintaining acid–base homeostasis. Our work established that taurine plays the essential role as pH buffering system (Fig. 8).

In order to demonstrate the effectiveness of the taurine buffering system *in vivo*,  $^{31}\text{P}$  MRS and proton MRS were used to investigate the brain's response to prolonged anoxia in rats post-natally. As summarized in Fig. 9, the one day old pup brain, which still maintains high concentrations of taurine, virtually identical to fetal brain, exhibits high acid buffering capability even under prolonged anoxia

and lactic acid formation, resulting in significant pH-lactate dissociation (Fig. 9A & B). In the ten day old pup brain, taurine contents are significantly reduced, and the pH buffering capacity is lost (Fig. 9C).<sup>10),14-20),23),24),26-28)</sup>

These findings provides the second conclusion: *High taurine concentration in fetal brain constitutes*

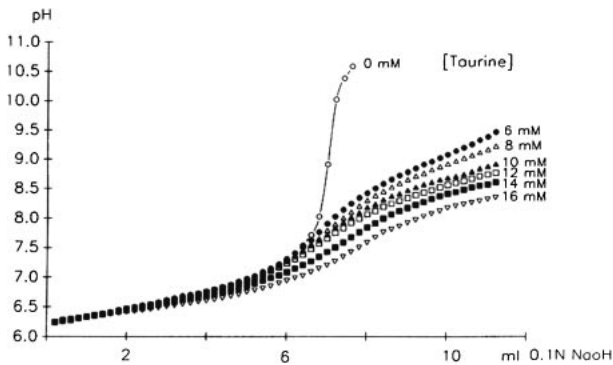


Fig. 8. Titration curve. Titration curves demonstrating the effects of the addition of taurine in various concentrations to a carbonate buffering system.

*an effective buffering system due to its high pKa value.*

**HEP diffusivity is facilitated in adult brain by the taurine-NAA exchange.** *In vivo* experimental data of HEP kinetics are summarized in Tables 1-3. HEP demand represented by  $K_f$  in adult brain is twice higher ( $0.26 \pm 0.03$ ) than that of the newborn pup ( $0.13 \pm 0.03$ ).<sup>21),22),29)</sup> In order to meet this significantly higher demand of energy consumption, diffusivity of HEP, the sole process of HEP transport from mitochondria to plasma membrane, is also significantly facilitated. Estimation of diffusion lengths revealed that the mean distance of HEP transport remains relatively constant, indicating that facilitation of diffusivity is quantitatively proportional to the increase in energy demand.

The cytosol represents a multi-component solution which contains small molecules such as electrolytes and free amino acids (taurine and NAA) as well as polymers such as proteins and nucleotides. In order to assess that the facilitation in HEP transport shown above is indeed the result of taurine-NAA exchange, the following mathematical modeling and

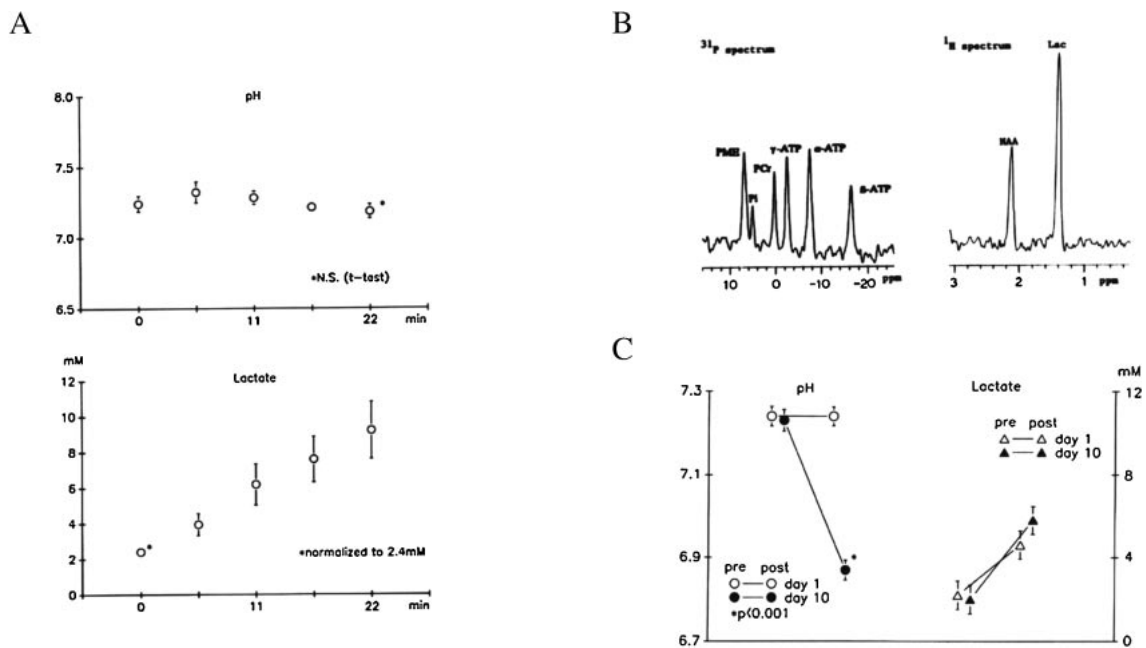


Fig. 9. pH-lactate dissociation in anoxic insult post-natally. A: Changes in intracellular pH and lactate levels of day 1 pup in response to anoxia. Mean and standard deviation ( $n = 10$ ). The pH value after 22 min of anoxia is not significantly different from normal controls, showing the remarkable capability of the 1 day old pup brain to preserve normal pH in spite of significant accumulation of lactate. B: representative  $^{31}\text{P}$  and proton spectra of 10 day old pup brain following 7.5 min of anoxia. PME: phosphomonoester, Pi: inorganic phosphate, PCr: phosphocreatine,  $\alpha$ -,  $\beta$ -,  $\gamma$ -ATP:  $\alpha$ -,  $\beta$ -,  $\gamma$ -adenosine triphosphate, NAA: N-acetyl-aspartate. C: Changes in intracellular pH and lactate levels of 1 day and 10 day old pups in response to 7.5 min of anoxia.

Table 1. Kinetic value for the forward reaction. mean  $\pm$  standard deviation, n = 6

	Ms/Mo	T <sub>1app</sub>	Kf (sec <sup>-1</sup> )
Newborn	0.78 $\pm$ 0.02	1.71 $\pm$ 0.05	0.13 $\pm$ 0.03
Adult	0.45 $\pm$ 0.04	2.12 $\pm$ 0.06	0.26 $\pm$ 0.03

Table 2. Diffusion coefficients. mean  $\pm$  standard deviation, n = 6

	PCr	ATP
Newborn	3.45 $\pm$ 0.89	2.95 $\pm$ 0.18
Adult	9.43 $\pm$ 0.83	6.38 $\pm$ 1.06

$\times 10^{-6}$  cm<sup>2</sup>/sec

Table 3. Life span and diffusion length

	Life time (sec)	Diffusion length ( $\mu$ m)*
PCr	Newborn	7.7
	Adult	3.8
ATP	Newborn	5.3
	Adult	1.8

\*mean  $\pm$  standard deviation, n = 6

simulation analysis was performed for multi-component diffusion.

The diffusivity of small molecules A,  $D_A$ , in an ideal solution at infinite dilution can be given by the Stokes-Einstein relation,

$$D_A = \frac{\tau}{6\pi\eta R_A}$$

where  $\tau$  is the fundamental temperature (4.28  $\times 10^{-14}$  ergs for a biological tissue temperature of 37°C),  $\eta$  is the viscosity of the solution, and  $R$  is the hydrodynamic radius of the molecule. The viscosity of an ideal solution is a function of the density of the solvent molecule:

$$\eta_s \propto \rho_s.$$

Assuming the density distribution of the micro-molecular substrate added to our model solution (taurine or NAA) is uniform, the viscosity of the solution can be treated as the linear sum of each solvent's viscosity and can be given by:

$$\eta = \eta_b + \eta_s,$$

where  $\eta_b$  and  $\eta_s$  are the viscosity of the base solution and substrate (taurine or NAA), respectively. Accordingly,  $D_A$  can be expressed by:

$$D_A = \frac{\tau}{6\pi R_A} \times \frac{1}{\eta_b + f_s \rho_s},$$

where,  $f_s$  is a contribution factor which is a function of various physicochemical variables, including the diffusivity of the substrate itself and activity coefficients. For the purpose of the biological modeling,  $f_s$  can be treated as constant for each substrate.

To minimize the errors of the Stokes-Einstein equation in multi-component diffusion where one of the components is a dilute polymer, Yam *et al.* introduced a mathematical model which involves a local viscosity function that combines diffusional hydrodynamics with Maxwell's treatment of electrical resistance in inhomogeneous regions.<sup>45)</sup> The diffusivities of small molecules in such a solution can be given by,

$$D_A = \frac{\tau}{6\pi\eta_0 R_A} \times B \\ = D_0 \times B,$$

where  $D_0$  is the diffusivity of the molecules in question in a polymerless solution and  $B$  is the effects of polymers given by,

$$B = \left( 1 + \frac{d \ln \gamma_A}{d \ln x_A} \right) \times \left[ \frac{2\eta_{pr} + \eta_0 - 2\Phi_{pr}(\eta_{pr} - \eta_0)}{2\eta_{pr} + \eta_0 + \Phi_{pr}(\eta_{pr} - \eta_0)} \right].$$

Here,  $\Phi_{pr}$  is the volume fraction of the polymer affected regions, and  $\eta_0$  and  $\eta_{pr}$  are the viscosities of the remaining solution and polymer affected regions, respectively. The model predicts experimental results far more accurately, and confirms that the high global viscosity brought about by polymers has only little effect on effective viscosity and, hence, the diffusivities of micromolecular solutes.

The viscosity of polymer affected regions is much higher than the viscosity of the remaining solution,  $\eta_{pr} \gg \eta_0$  and therefore, by treating the activity terms as the constant  $A_c$ ,  $B$  can be vigorously simplified for the purpose of biological modeling to:

$$B \cong A_c \times \left[ \frac{2 - 2\Phi_{pr}}{2 + \Phi_{pr}} \right].$$

Using the experimental data of Yam *et al.*,  $\Phi_{pr}$  can be approximated by,

$$\Phi_{pr} \cong 4\Phi_p \\ \cong \frac{0.004c}{0.8 + 0.01c},$$

where  $\Phi_p$  is the volume fraction of polymers and  $c$  is the polymer concentration in w/v% (gram per 100 ml). Accordingly, a very simplified equation for

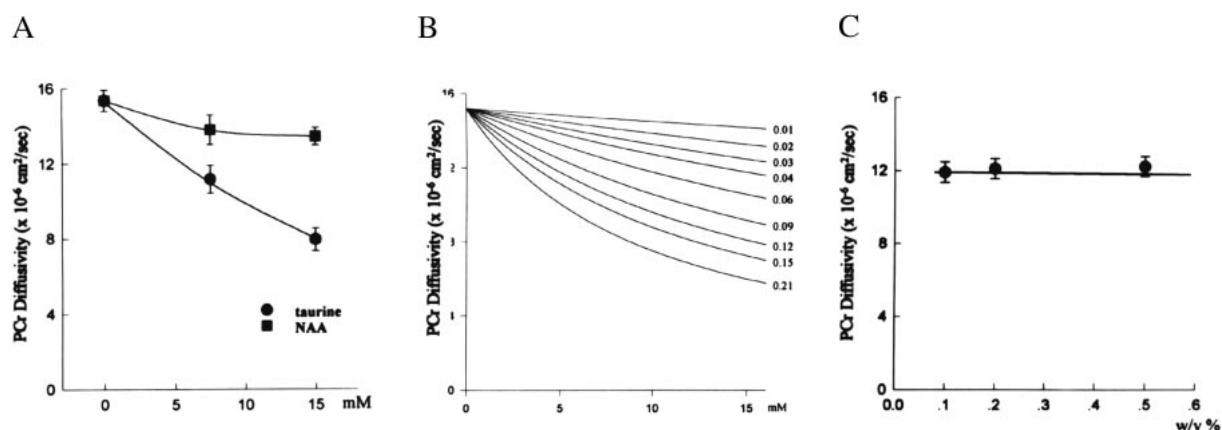


Fig. 10. Diffusivity analysis.

A: PCr diffusivity in a taurine or NAA containing model solution. Mean  $\pm$  standard deviation ( $n = 5$ ). Solid line indicate the theoretical curve using the equation described in the test with  $f_s$  values of 0.14 and 0.02 for taurine and NAA, respectively.

B: Standard curve for  $f_s$  value determination generated using the equation described in the test.

C: PCr diffusivity in an albumin containing model solution. Mean  $\pm$  standard deviation ( $n = 5$ ). Solid line indicates the theoretical curve using the equation described in the text. There is excellent agreement with experimental data, confirming that biopolymers have only negligible effects on PCr diffusivity over a large range of concentrations.

the diffusivities of small molecule in a polymer containing solution as a function of polymer concentration can be given by,

$$D_A = D_0 \times A(c) \times \frac{1.6 - 0.02c}{1.6 + 0.02c} \quad (c \geq 0)$$

$$A(c) = \begin{cases} 1 & (c = 0) \\ A_c & (c > 0) \end{cases}$$

The function  $A(c)$  is introduced to emphasize that the activity term is dependent on the presence of polymers.

PCr diffusivity in a model solution containing various concentrations of taurine or NAA is measured and summarized in Fig. 10A. It is apparent that changes in the concentration of taurine have a significantly greater effect on PCr diffusivity than NAA.

The value of  $\eta_b$  for PCr in the model solution can be determined for the condition  $\rho_s = 0$ . Using  $D_A = 15.3 \times 10^{-6} \text{ cm}^2/\text{sec}$ ;  $R_A = 0.7 \text{ nm}$ ;  $\tau = 4.11 \times 10^{-14} \text{ ergs}$  at  $25^\circ\text{C}$ ,  $\eta_b$  was estimated to be  $2.04 \times 10^{-3} \text{ g/cm-sec}$ . Accordingly, diffusivity of PCr ( $\times 10^{-6} \text{ cm}^2/\text{sec}$ ) in the model solution,  $D_{PCr}$ , can be rewritten as:

$$D_{PCr} = \frac{31}{2.04 + f_s \rho_s}$$

where  $\rho$  is expressed as mM concentration. Computer generated standard curves for various  $f_s$  values is shown in Fig. 10B. Taurine and NAA solutions correlate to  $f_s$  values of 0.14 and 0.02, respectively.

The effects of albumin on PCr diffusivity are

summarized in Fig. 10C. Despite the fivefold change in albumin concentration (0.1 to 0.5 w/v%), PCr diffusivity remains rather constant, confirming that PCr indeed behaves as micromolecule in a polymer-containing solution as discussed in the Theory section. The results indicate that biological polymers (proteins, lipids, nucleic acids) are indeed likely to have little effect, if any, on the *effective viscosity* of cytosol.

PCr diffusivity in a solution without biopolymers (albumin) was  $15.3 \pm 0.56$ , whereas PCr diffusivity in a solution with albumin (0.1% w/v) was  $11.9 \pm 0.33$ . Given that PCr diffusivity differences are primarily due to thermodynamic effects of polymers on PCr and, hence, reflect the activity term  $A_c$ , the value of  $A_c$  can be estimated by taking their ratio and was found to be 0.78. Accordingly, using the value of PCr diffusivity in water as  $D_0$  value,  $D_{PCr}$  can be given by:

$$D_{PCr} = 15.3 \times A(c) \times \frac{1.6 - 0.02c}{1.6 + 0.02c} \quad (c \geq 0)$$

$$A(c) = \begin{cases} 1 & (c = 0) \\ 0.78 & (c > 0) \end{cases}$$

A computer generated theoretical curve using this equation for  $c > 0$  is shown in Fig. 10C as a solid line and is in excellent agreement with experimental data, confirming that biopolymers have only negligible effects on PCr diffusivity over a large range of concentrations.

Considering a cytosolic environment where taurine and NAA coexist, cytosolic viscosity can be expanded into three terms:

$$\eta = \eta_w^* + f_{\text{tau}}^* \rho_{\text{tau}} + f_{\text{naa}}^* \rho_{\text{naa}}$$

Where asterisk signifies *in vivo* conditions. Taking into account the presence of biopolymers in cytosol and the activity term, PCr diffusivity in cytosol can be expressed by:

$$D_{\text{PCr}}^* = \frac{\tau}{6\pi R_A} \times \frac{A_c^*}{\eta_b^* + f_{\text{tau}}^* \rho_{\text{tau}} + f_{\text{naa}}^* \rho_{\text{naa}}}$$

Using the *in vitro* data described above for approximation of *in vivo* conditions,  $D_{\text{PCr}}^*$  can be approximated by:

$$D_{\text{PCr}}^* = \frac{24}{2.04 + 0.14\rho_{\text{tau}} + 0.02\rho_{\text{naa}}}$$

and PCr diffusivity in newborn pup brain with 16 mM of taurine and 1 mM of NAA is estimated to be  $5.58 \times 10^{-6} \text{ cm}^2/\text{sec}$ . Similarly, PCr diffusivity in adult brain with 4 mM of taurine and 7 mM of NAA is estimated to be  $9.95 \times 10^{-6} \text{ cm}^2/\text{sec}$ . The values are in excellent agreement with the experimental data summarized in Table 2.

These findings provide the third conclusion: *High energy phosphate (HEP) transport from mitochondria to cell membrane is effected through the passive diffusion of HEP in the cytosol and is significantly facilitated by replacement of taurine by NAA.*

### Conclusion

The brain undergoes significant adjustments from fetal to adult life, the most obvious of which is in its need to meet the drastic increase in energy consumption at the neuronal cell membrane due to the explosive increase in neural activities after birth. Actual changes were found to be taken place in two systems, namely, acid base balance control and cytosolic energy transport. The adjustments are accomplished by converting cytosol microenvironment from a taurine rich fetal type environment to an N-acetyl-aspartate (NAA) rich adult type environment during the post-natal period. High concentrations of taurine are necessary to provide effective buffering in the fetal brain, because the fetus cannot utilize the adult type of  $\text{pCO}_2$  dependent acid-base balance control system, namely respiration driven  $\text{pCO}_2$  changes. To accommodate the significantly higher demand of energy consumption at the membrane due to the increased neuronal activities,

taurine has to be replaced by NAA, since the latter facilitates HEP transport from mitochondria to the membrane by passive diffusion.

### Acknowledgment

The study was supported by grants from the NIH, Department of Veterans Affairs Research Service, the Ministry of Education, Culture, Sports, Science, and Technology (Japan), and University of Niigata.

### References

- 1) Jones, C.T. (1982) *The Biochemical Development of the Fetus and Neonate*. Elsevier Biomedical Press, Amsterdam.
- 2) Hoult, D.I., Busby, S.J.W., Gadian, D.G., Radda, G.K., Richards, R.E. and Seeley, P.J. (1974) Observation of tissue metabolites using  $^{31}\text{P}$  nuclear magnetic resonance. *Nature* **252**, 285–287.
- 3) Ackerman, J.J.H., Grove, T.H., Wong, G.G., Gadian, D.G. and Radda, G.K. (1980) Mapping of metabolites in whole animals by  $^{31}\text{P}$  NMR using surface coils. *Nature* **283**, 167–170.
- 4) Prichard, J.W., Alger, J.R., Behar, K.L., Petroff, O.A.C. and Shulman, R.G. (1983) Cerebral metabolic studies *in vivo* by  $^{31}\text{P}$  NMR. *Proc. Natl. Acad. Sci. USA* **80**, 2748–2751.
- 5) Nakada, T., Kwee, I.L., Miyazaki, T., Iriguchi, N. and Maki, T. (1987)  $^{31}\text{P}$  *in vivo* spectroscopy of the stomach by zig-zag coil. *Magn. Reson. Med.* **5**, 449–455.
- 6) Kwee, I.L. and Nakada, T. (1988) Regional phospholipid profile of the human brain:  $^{31}\text{P}$  NMR spectroscopic study. *Magn. Reson. Med.* **6**, 296–299.
- 7) Nakada, T., Kwee, I.L. and Rao, G.A. (1988) Phospholipid profile of the developing brain:  $^{31}\text{P}$  NMR spectroscopic study in rat pups. *Biochem. Arch.* **4**, 35–40.
- 8) Nakada, T. (1989) Biomedical NMR spectroscopy: Past, present and future. *Med. Imaging Tech.* **7**, 115–125.
- 9) Houkin, K., Nakada, T., Suzuki, N. and Kwee, I.L. (1989) Cortical spectroscopy: Localized spectroscopy of the cerebral cortex in rats. *Magn. Reson. Med.* **12**, 364–368.
- 10) Nakada, T., Kwee, I.L., Suzuki, N. and Houkin, K. (1989) Intrauterin fetal brain NMR spectroscopy:  $^1\text{H}$  and  $^{31}\text{P}$  studies in rats. *Magn. Reson. Med.* **12**, 172–180.
- 11) Houkin, K., Nakada, T., Suzuki, N. and Kwee, I.L. (1989)  $^{31}\text{P}$  Magnetic resonance spectroscopy of chronic infarction in rats. *NMR Biomed.* **2**, 83–86.
- 12) Nakada, T. (1990) Magnetic resonance spectroscopy in the study of brain metabolism: New horizon for clinical neurology. *Hospimedica* **8**, 51–55.
- 13) Houkin, K., Kwee, I.L. and Nakada, T. (1990) Persistent high lactate, the most sensitive NMR spectroscopic indicator of completed infarction. *J. Neurosurg.* **72**, 763–766.
- 14) Nakada, T. (1991) Brain maturation and acid-base

- balance: Taurine/N-acetyl-aspartate replacement hypothesis (eds. Niimi, H., Hori, M., Naritomi, H.). Microcirculatory Disorder in the Heart and Brain. Harwood Academic Publishers, Philadelphia, pp. 175–188.
- 15) Nakada, T., Houkin, K., Hida, K. and Kwee, I.L. (1991) Rebound alkalosis and persistent lactate: Multinuclear ( $^1\text{H}$ ,  $^{13}\text{C}$ ,  $^{31}\text{P}$ ) NMR spectroscopic study. *Magn. Reson. Med.* **18**, 9–14.
  - 16) Kwee, I.L., Nakada, T. and Suzuki, N. (1991)  $^{31}\text{P}$  and 3-FDG  $^{19}\text{F}$  NMR spectroscopy of aged brain in rats. *NMR Biomed.* **4**, 38–40.
  - 17) Suzuki, N., Kwee, I.L. and Nakada, T. (1991)  $^{31}\text{P}$  Nuclear magnetic resonance spectroscopy of 9L gliosarcoma cell line: Differential effects of chemotherapy in spheroid and anchored culture. *Magn. Reson. Med.* **19**, 422–428.
  - 18) Kwee, I.L., Nakada, T. and Ellis, W.G. (1991) Elevation in relative levels of brain membrane unsaturated fatty acids in Alzheimer's disease: High resolution proton spectroscopic studies of membrane lipid extracts. *Magn. Reson. Med.* **21**, 49–54.
  - 19) Hida, K., Suzuki, N., Kwee, I.L. and Nakada, T. (1991) pH-lactate dissociation in neonatal anoxia: proton and  $^{31}\text{P}$  NMR spectroscopic studies in rat pups. *Magn. Reson. Med.* **22**, 128–132.
  - 20) Nakada, T., Hida, K. and Kwee, I.L. (1991) pH-lactate dissociation during anoxic insult: Taurine effect. *Neuroreport* **2**, 325–328.
  - 21) Nakada, T. and Kwee, I.L. (1991) Maturation changes in intracellular high energy phosphate diffusivity in rat brain. *Neuroreport* **2**, 777–780.
  - 22) Nakada, T. (1992) Investigational methodologies for the effect of brain maturation on cellular energy transport. *Keio J. Med.* **41**, 64–67.
  - 23) Hida, K., Kwee, I.L. and Nakada, T. (1992) *In vivo*  $^1\text{H}$  and  $^{31}\text{P}$  NMR spectroscopy of the developing rat brain. *Magn. Reson. Med.* **23**, 31–36.
  - 24) Suzuki, N., Kwee, I.L. and Nakada, T. (1992) Brain maturation and response to anoxia:  $^{31}\text{P}$  NMR spectroscopic studies in rat pups. *Magn. Reson. Med.* **24**, 205–211.
  - 25) Hida, K., Kwee, I.L. and Nakada, T. (1992) T1 values of phosphomonoester and phosphocreatine of the brain show no significant change during development. *Magn. Reson. Med.* **27**, 179–182.
  - 26) Nakada, T., Hida, K. and Kwee, I.L. (1992) Brain pH and lactic acidosis: Quantitative analysis of taurine effect. *Neurosci. Res.* **15**, 115–123.
  - 27) Nakada, T. and Kwee, I.L. (1993)  $^{31}\text{P}$  Localized spectroscopy of fetal brain in utero. *Magn. Reson. Med.* **29**, 122–124.
  - 28) Nakada, T. and Kwee, I.L. (1993) Guanidinoethane sulfate: Brain pH alkaline shifter. *Neuroreport* **4**, 1035–1038.
  - 29) Nakada, T., Kwee, I.L. and Igarashi, H. (1994) Brain maturation and high energy phosphate diffusivity: Alteration in cytosolic microenvironment and effective viscosity. *Dev. Brain Res.* **80**, 121–126.
  - 30) Sturman, J.A., Rassin, D.K. and Gaull, G.E. (1977) Taurine in developing rat brain: maternal fetal transfer of  $\{^{35}\text{S}\}$ taurine and its fate in the neonate. *J. Neurochem.* **28**, 31–39.
  - 31) Huxtable, R.J. (1989) Taurine in the central nervous system and the mammalian actions of taurine. *Prog. Neurobiol.* **32**, 471–533.
  - 32) Lawson, J.W.R. and Veech, R.L.J. (1979) Effects of pH and free  $\text{Mg}^{2+}$  on the  $K_{eq}$  of creatine kinase reaction and other phosphate hydrolyses and phosphate transfer reactions. *J. Biol. Chem.* **254**, 6528–6537.
  - 33) Bessman, S.P. and Geiger, P.J. (1981) Transport of energy in muscle. *Science* **211**, 448–452.
  - 34) Degani, H., Alger, J.R., Shulman, R.G., Petroff, O.A.C. and Prichard, J.W. (1987)  $^{31}\text{P}$  magnetization transfer studies of creatine kinase kinetics in living rabbit brain. *Magn. Reson. Med.* **5**, 1–12.
  - 35) Shoubridge, E.A., Briggs, R.W. and Radda, G.K. (1982)  $^{31}\text{P}$  NMR saturation transfer measurements of the steady state rates of creatine kinase and ATP synthetase in the rat brain. *FEBS Lett.* **140**, 288–292.
  - 36) Brown, T.R. and Ogawa, S. (1977)  $^{31}\text{P}$  nuclear magnetic resonance kinetic measurements on adenylate kinase. *Proc. Natl. Acad. Sci. USA* **74**, 3627–3631.
  - 37) Alger, J.R. and Shulman, R.G. (1984) NMR studies of enzymatic rats *in vitro* and *in vivo* by magnetization transfer. *Q. Rev. Biophys.* **17**, 83–124.
  - 38) Kittel, C. and Kroemer, H. (1980) *Thermal Physics*. W. H. Freeman and Company, New York.
  - 39) Arfken, G. (1985) *Mathematical Methods for Physics*. Academic Press, New York.
  - 40) Stejskal, E.O. and Tanner, J.E. (1965) Spin diffusion measurements: spin-echoes in the presence of a time-dependent field gradient. *J. Chem. Phys.* **42**, 288–292.
  - 41) Carr, H.Y. and Purcell, E.M. (1954) Effects of diffusion on free precession in nuclear magnetic resonance experiments. *Phys. Rev.* **94**, 630–635.
  - 42) Nakada, T., Nakayama, N., Fujii, Y. and Kwee, I.L. (1999) Clinical application of magnetic resonance axonography. *J. Neurosurg.* **90**, 791–795.
  - 43) Nakada, T., Matsuzawa, H., Fujii, Y., Takahashi, H., Nishizawa, M. and Kwee, I.L. (2006) Three dimensional anisotropy contrast periodically rotated overlapping parallel lines with enhanced reconstruction (3DAC PROPELLER) on a 3.0T system: A new modality for routine clinical neuroimaging. *J. Neuroimaging* **16**, 206–211.
  - 44) Tallan, H.H. (1957) Studies on the distribution of N-acetyl-L-aspartic acid in brain. *J. Biol. Chem.* **22**, 41–45.
  - 45) Yam, K.L., Anderson, D.K. and Buxbaum, R.E. (1988) Diffusion of small solutes in polymer-containing solutions. *Science* **241**, 330–332.

(Received Jan. 22, 2010; accepted Apr. 27, 2010)

## Profile

Tsutomu Nakada received his M.D. (Medicine) and Ph.D. (Biomedical NMR) from University of Tokyo. After completion of his clinical training at University of Tokyo, University of California (San Francisco and Davis), and Stanford University, he became an Assistant Professor of Neurology at University of California, Davis, in 1982. Subsequently, he was promoted to Associate Professor in 1988 and Professor in 1992. In 1996, he was recruited to establish a new research center at the Brain Research Institute, University of Niigata, where he currently holds professorship and directorship. He is board certified in Internal Medicine (Japan), Neurology (Japan and USA), Clinical Neurophysiology (USA), and Imaging (USA). He was elected to fellow of the American Academy of Neurology in 1988 and council member of the Science Council of Japan in 2008.

